Numerical investigation towards HiTAC conditions in laboratory-scale ethanol spray combustion

Zhu, Shanglong; Pozarlik, Artur; Roekaerts, Dirk; Rodrigues, Hugo Correia; van der Meer, Theo

DOI
10.1016/j.fuel.2017.09.002

Publication date
2018

Document Version
Final published version

Published in
Fuel: the science and technology of fuel and energy

Fuel 211 (2018) 375–389

Contents lists available at ScienceDirect

Fuel

journal homepage: www.elsevier.com/locate/fuel

Full Length Article

Numerical investigation towards HiTAC conditions in laboratory-scale ethanol spray combustion

Shanglong Zhu[a,*], Artur Pozarlik[a], Dirk Roekaerts[b], Hugo Correia Rodrigues[b], Theo van der Meer[a]

[a] Laboratory of Thermal Engineering, University of Twente, The Netherlands
[b] Department of Process and Energy, Delft University of Technology, The Netherlands

ARTICLE INFO

Keywords:
HiTAC
Hot co-flow
Ethanol
Spray combustion

ABSTRACT

In the past 25 years high temperature air combustion (HiTAC) technology has been proved and utilized in industry as a promising way to increase thermal efficiency, create a relatively uniform temperature distribution, and reduce emissions of harmful pollutants such as NO_X and CO. However, due to the complexity of fuel-oil combustion, to date HiTAC is mainly applied to gaseous fuel or coal, and little is known about spray combustion under HiTAC condition. In the present study, we numerically investigate the Delft Spray-in-Hot-Coflow (DSHC) using ethanol in high temperature diluted combustion air, and extend it to more co-flow conditions. We employ different temperatures and oxygen concentrations of the co-flow in order to dilute the oxidizer/fuel before it reacts with the fuel/ oxidizer. The pressure-swirl atomizer model with an Eulerian-Lagrangian approach was implemented for the spray modeling. Collision, coalescence, secondary breakup and evaporation of the drops were taken into account. The steady laminar flamelet model for the combustion of ethanol, the Discrete Ordinate model for radiation and the k-ε model for the turbulence with enhanced wall treatment were validated by the simulation of the NIST flame under conventional conditions and then used in the current study.

The results indicate that the decreased peak temperature in many HiTAC applications with high temperature combustion air is mainly due to the reduced oxygen concentration by entraining flue gas.

In the present study, a low oxygen concentration slows the evaporation process of droplets. It results in an enlarged combustion zone, a lowered peak temperature and minor NO_X emission. However, decreasing the oxygen concentration may lead to problems of cracking, soot formation and flame extinction, especially for heavy oils. The optimization needs to be carried out based on the analysis of a specific fuel in order to create a HiTAC-like condition.

Based on the results of the current study, the 1500 K and 6%vol oxygen concentration case is considered as a HiTAC condition.

1. Introduction

High temperature air combustion (HTAC) is a promising technology for energy saving, flame stability enhancement and reduction of NO_X emission. It has been applied in many experimental and industrial applications, and also developed and reported as “moderate or intense low oxygen dilution (mild) combustion”, “flameless oxidation”, or “colorless distributed combustion (CDC)” [1–8]. In such a combustion regime, oxygen/fuel stream is diluted by a substantial amount of hot inert flue gases before it reacts with the fuel/oxygen. This results in more uniform temperature distribution and lower NO_X emission than in case of conventional combustion. To date most of the applications of HiTAC are for gaseous fuels [3–5] or solid fuels [9,10], but little is known about spray combustion under HiTAC condition [1,11]. H. Tsuji et al. [1] introduced the historical background of HiTAC technology, and described its development and practical application to different kinds of furnaces of importance in industry. Besides the gaseous and solid fuels, they investigated experimentally kerosene spray flames and reported qualitatively with photographs the states of spray flame combustion in the high temperature preheated diluted air (523 K to 1373 K), when the O_2 concentration is changed (13% to 3%), Although it was concluded that NO_X emissions reduce in the same manner as gaseous fuel, cases when the O_2 concentration in highly preheated air is lower than 15% were not further discussed. Moreover, the experimental results from NKK Keihin using heavy oil A did not show a clear trend [1]. That can be explained by the complexity of spray combustion and many unclear fundamental aspects involved in spray combustion, in particular turbulent spray combustion. Modeling of turbulent spray combustion

* Corresponding author.
E-mail address: zhushanglong@gmail.com (S. Zhu).

http://dx.doi.org/10.1016/j.fuel.2017.09.002
Received 9 May 2016; Received in revised form 17 February 2017; Accepted 5 September 2017

however, although challenging provides a better understanding of various phenomena in the processes involved. In a real turbulent spray flame, dispersion, continuous phase turbulence modification, dispersed phase inter-particle collisions, evaporation, mixing and combustion occur simultaneously. Dealing with all these complexities and their interactions poses a tremendous modeling task [11]. Jenny et al. [11] reviewed the modeling developments of turbulent spray combustion, together with the relevant experiments of spray flame configurations presented in a structured way, with the intention to provide a database for model validation and a guideline for future investigations. The ethanol spray flame modeling presented in the current study is one of the investigations using the Delft Spray-in-Hot-Coflow (DSHC) burner.

To address all the relevant phenomena, we employ a combination of models, such as models for turbulence, atomization, secondary break-up, collision and coalescence, evaporation, radiative heat transfer, combustion, etc. These models have been validated already by the simulation of the NIST flame using methanol under conventional condition [12] and then were applied for comparison with preliminary results from the ethanol spray-in-hot-co-flow [13]. The predicted mean velocity components of the gaseous flow and the droplets, the droplet number density, and the Sauter mean diameter (SMD) of the droplets at various heights showed good agreement with the experimental data. The method to set inlet boundary conditions for the spray has been discussed and compared with direct application of data regarding measured droplet size and velocity distribution. In the application for modeling the ethanol spray-in-hot-co-flow case, relatively good agreement with experimental data of mean droplet velocity components and size distribution at various elevations has been observed, as well. It was recommended that under hot co-flow conditions, the evaporation model and the auto-ignition and local extinction processes require more efforts in order to obtain more accurate prediction in the high strain region, which is in the vicinity of the injector exit. Ma et al. [14,15] further exploited more directly all available measured data and used a “conditional droplet injection model”, in which large droplets are injected within a small range of angle around the main spary trajectory while small droplets are injected in a much wider range. In this way the prediction of SMD in low droplet number density region also showed good agreement with the experimental data, as well as in the vicinity of the injector exit.

However, with the DSHC setup, the co-flow temperature and oxygen dilution cannot be varied independently [16]. As a result, the temperature, velocity of gas and liquid, gas components in the co-flow and their distribution vary depending on the investigated test case. Furthermore, due to the performance of the atomizer under different co-flow temperature conditions, the mass flow of ethanol can be different from the designed one. This can be verified by the reported injection pressure and mass flow rate of ethanol [17]. As a result, in order to investigate the influential parameters on combustion characteristics, we focus on a comparative numerical study of cases with different co-flow temperatures and O_2 concentrations using the validated models in a wider range than studied experimentally.

In the present research, we used different co-flow temperatures (300 K, 600 K, 900 K, 1200 K and 1500 K) and oxygen concentrations (21%, 18%, 15%, 12%, 9% and 6%) of the co-flow. The mass flow rate and pressure of the fuel-oil are kept constant. The simulation results from different cases, such as temperatures, flame profiles, droplet size distributions, etc., are studied with respect to HiTAC conditions.

As we discussed in [12], both the boundary condition and spray trajectory analysis are essential for validation of spray flames. The validation of the DSHC ethanol spray flame requires both a well-defined boundary condition of co-flow and a detailed analysis of spray trajectory. To clearly identify the influence of temperature and oxygen concentration in the coflow we here study two typical operation conditions of DSHC test rig, i.e. cold co-flow condition (300 K, 21% vol O_2) and hot co-flow condition (1500 K, 6% vol O_2), keeping the composition of the rest of the coflow identical. They represent spray flames under conventional condition and towards-HiTAC condition, respectively.

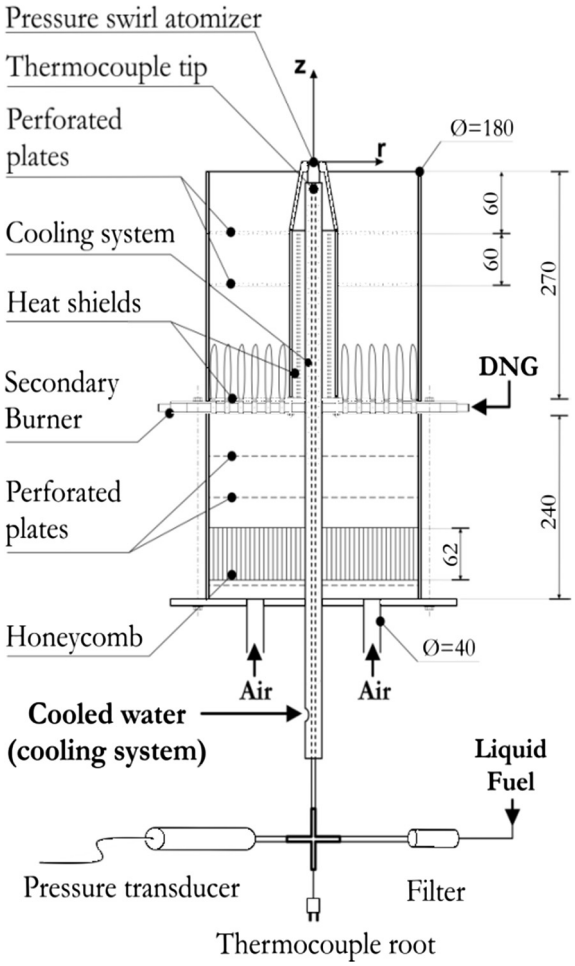

Fig. 1. Schematic of the Delft spray flame set-up (mm).

2. Numerical cases

The numerical cases are based on the experimental set up available at Delft University of Technology using the DSHC burner. Fig. 1 presents a schematic of the Delft spray burner [17,18]. An ethanol spray is produced by a pressure swirl atomizer, whereas the hot co-flow is assured by secondary burner whereby air and Dutch natural gas (DNG) mix and generate a matrix of 236 lean flames. The air/DNG ratios in combination with the effects of two perforated plates located along the pipe length dictate the temperature, oxygen and turbulence levels. Co-flow composition and temperature are selected to emulate the conditions of flue gas in large scale furnaces. This design enables a wide range of co-flow characteristics with good axisymmetric properties without the need for elaborate safety systems and allows easy optical access to laser diagnostics.

3. Mathematical models

The mathematical formulation for turbulent spray combustion simulation consists of the consideration of the computational grid, turbulence model, spray model, radiation and combustion model, NO_X model etc. Since these models and methods are expected to be validated and developed to generate the knowledge needed for the extension of the application of HiTAC technology to other fuel oils in various applications, for which detailed reaction mechanisms may still need to be investigated and various geometries of chambers/furnaces may be involved, the Reynolds averaged equations are employed, using ANSYS Fluent software. As a result, the models used in the study remain as general as possible in order to be implemented for various applications.

3.1. Computational grid, near-wall treatment and turbulence model

For the simulation of the Delft spray flame, a 2D axisymmetric simulation is employed. The grid independence was tested by introducing a series of different cell sizes. The same axial/radial aspect ratio of 3 was kept in order to avoid the interference of potential errors caused by the aspect ratio. A considerable larger aspect ratio however leads to large cells close to the outlet which reduces the accuracy of results, while a considerable lower aspect ratio enhances the amount of cells requiring unnecessary computational cost. The role of the near-wall treatment was analyzed, and a 2D mesh with about 0.6 million quadrilateral cells in combination with the second order upwind scheme was found suitable for this study. A standard k-ε turbulence model with the enhanced wall treatment is applied based on the comparative analysis. The use of the enhanced wall treatment can possess the accuracy of the standard two-layer (a viscosity affected region and a fully-turbulent region) approach for the fine near-wall mesh and at the same time, not reducing accuracy for the wall-function mesh.

3.2. Spray model

In spray combustion studies, often the focus is on the modelling of dilute spray combustion due to the complexity of the processes of injection and atomization [11,19]. The experimental data of droplets, i.e. velocity components and size distribution, are frequently used as boundary conditions. Those data are supposed to be measured at a certain axial location, where the atomization has already finished while the injected droplets have not been influenced by the airflow and only a minor part of the evaporation has occurred. However, on one hand, the measurement technique provides data on only part of the liquid flux close to the atomizer; on the other hand, at further downstream positions, the droplets have already interacted with the co-flow, especially in hot co-flow, and boundary conditions on droplets have to be complemented with boundary conditions on vapor concentration and gas velocity [12]. As a result, we here keep using the Linearized Instability Sheet Atomization (LISA) model to simulate the transition of ethanol from the internal injector flow to fully developed spray by a pressure-swirl atomizer [12,20]. In this model Kelvin-Helmholtz waves grow on the sheet and eventually break the liquid into ligaments which are further break up into droplets due to varicose instability. The film formation follows the below relationship:

$$\dot{m}_{eff} = \pi \rho u t (d_{inj} - t) \tag{1}$$

where t is the thickness of the film, $\cdot m_eff$ is the effective mass flow rate, d_{inj} is the injector exit diameter, and u is the mean axial component of velocity at the injector exit. The approach of Han et al. [21] is used to calculate the velocity magnitude of u:

$$U = k_v \sqrt{\frac{2\Delta P}{\rho_l}} \tag{2}$$

where k_v is a dimensionless velocity coefficient and a function of the injector design and injection pressure [22]. If the pressure difference at the injector, ΔP is known, u can be calculated as

$$u = U \cos\theta \tag{3}$$

where θ is the spray angle.

The effects of the surrounding gas, liquid viscosity and surface tension on the breakup of the liquid sheet are also included in the LISA model for sheet breakup and atomization, which is based on the growth of sinusoidal waves on the liquid sheet.

The breakup from ligaments to droplets is assumed to occur according to Weber's analysis for capillary instability [23]. So the most probable diameter for droplet diameter distribution, d_0, is determined from:

$$d_0 = 1.88 d_L (1 + 3Oh)^{1/6} \tag{4}$$

where oh is the Ohnesorge number which is a combination of the Reynolds number and the Weber number.

Once this most probable droplet size has been found, with a spread parameter and a dispersion angle, the droplet diameter distribution is determined by a Rosin-Rammler distribution. According to our previous investigation [12], a spread parameter of 3.5 and a dispersion angle of 10° are found suitable for such a spray modelling using one main trajectory of spray injection.

In many real applications, there may arise need for a few trajectories to be superimposed in order to resemble better the real droplet diameter distribution and droplet velocity. Moreover, even with the same injector, the droplet diameter distribution and droplet velocity vary due to thermal expansion of the injector under various operating conditions. This makes the validation challenging. On one hand, even if there are experimentally measured data of droplets, in the vicinity of the injector they are often inadequate for a complete set of droplet diameter distribution and droplet velocity, which means they have to be tuned and verified by data at downstream elevations. On the other hand, even if well-tuned droplet diameter distribution and droplet velocity for one case are obtained and have been verified by data at downstream positions, they have to be tuned and verified again if the operating condition varies, especially when the measured data are directly used [12].

In the present study, however, we assume that the droplet size distribution and droplet velocity from the injector keep the same in various cases. This allows us for the comparative investigation of the influence of only the co-flow conditions.

In the simulation, the fuel is assumed to be injected into the chamber as a fully atomized spray consisting of spherical droplets of various sizes. The motion of the droplets in the turbulent combustion flow field are calculated using a stochastic method. The equation of motion for one droplet is:

$$\frac{du_{p,i}}{dt} = \frac{18\mu}{\rho_p D_p^2} \frac{C_D \mathrm{Re}}{24} (U_i - u_{p,i}) + \frac{g_i(\rho_p - \rho)}{\rho_p} + F_i \tag{5}$$

In this equation, $u_{p,i}$ is the velocity of droplet (particle) i, U is a sampled gas velocity, μ is the molecular viscosity of the fluid, ρ is the fluid density, ρ_p is the density of the particle, D_p is the particle diameter, Re is the relative Reynolds number based on slip velocity and particle diameter, and the drag coefficient C_D is a function of the particle Reynolds number. F_i is a possible additional acceleration term. In practice a number of 'parcels', each representing a set of identical droplets, is tracked.

The Taylor Analogy Breakup (TAB) model is used for secondary breakup. It is based upon Taylor's analogy [24] between an oscillating and distorting droplet.

The algorithm of O'Rourke [25] is employed for droplet collision and coalescence. It uses the concept of a collision volume to calculate the probability of collision. In general, once two parcels collide, the outcome tends to be coalescence if they collide head-on, and bouncing if the collision is more oblique. The critical offset for the probability of coalescence is a function of the collisional Weber number and the relative radii of the collector and the smaller droplet.

The rate of vaporization is governed by gradient diffusion, with the flux of droplet vapour into the gas phase related to the difference in vapor concentration at the droplet surface and the bulk gas:

$$N_i = k_c (C_{i,s} - C_{i,\infty}) \tag{6}$$

where N_i is the molar flux of vapour, C_i,s is the vapour concentration at the droplet surface, and C_i, is the vapour concentration in the bulk gas. K_c is the mass transfer coefficient calculated from the Sherwood number correlation [26,27], defined as:

$$Sh_{AB} = \frac{k_c D_p}{D_{i,m}} = 2.0 + 0.6 \mathrm{Re}^{1/2} Sc^{1/3} \tag{7}$$

where D_i,m is the diffusion coefficient of vapour in the bulk, Sc is the Schmidt number. The concentration of vapour at the droplet surface is evaluated by assuming that the partial pressure of vapour at the interface is equal to the saturated vapour pressure, P_sat, at the droplet temperature, T_p:

$$C_{i,s} = \frac{p_{sat}(T_p)}{RT_p} \tag{8}$$

where R is the universal gas constant.

3.3. Radiation and combustion model

In this study, the Discrete Ordinates (DO) radiation model with a variable absorption coefficient, weighted-sum-of-gray-gases model (WSGGM) is employed, which has been discussed in [1] and validated in our previous investigation [12].

According to the relative fast chemistry of ethanol, the laminar flamelet method provides a feasible way to include detailed chemical reactions in turbulent combustion simulations without a considerable increase in computational time. It assumes that in the gaseous phase combustion, the diffusion coefficients for all species are equal, and then the species mass fraction and temperature are mapped from physical space to mixture fraction space and can be uniquely described by two parameters: the mixture fraction ξ and the scalar dissipation rate χ. The Favre-averaged values of quantities in the turbulent flame are then obtained through the use of Favre-averaged probability density function, $\widetilde{f}(\xi,\chi)$:

$$\widetilde{\Phi} = \int_0^\infty \int_0^1 \Phi(\xi,\chi)\widetilde{f}(\xi,\chi)d\xi d\chi \tag{9}$$

The detailed reaction mechanism for ethanol employed in the present study was developed by Marinov [28] consisting of 57 species and 383 reactions.

In the model, the heat gain/loss to the system is assumed to have a negligible effect on the species mass fractions, and adiabatic mass fractions are used [29,30]. The flamelet profiles are then convoluted with the assumed PDF as in Eq. (9), and then tabulated for look-up. Assuming that fluctuations of scalar dissipation rate can be neglected, only the mean value has to be considered in Eq. (9) and the relevant PDF is the PDF of mixture fraction which is assumed to be a β-function. The equations for the mean mixture fraction, mixture fraction variance, and mean enthalpy are solved. The mean scalar dissipation field is calculated from the turbulence fields $\widetilde{k}$, $\widetilde{\varepsilon}$ and the mixture fraction variance $\widetilde{\xi}^{Prime2}$ as follows:

$$\widetilde{\chi} = \frac{2\widetilde{\varepsilon}\widetilde{\xi}''^2}{\widetilde{k}} \tag{10}$$

The mean values of temperature, density, and species mass fraction are obtained from the PDF look-up table. It should be pointed out that the β-function assumption in case of spray flames is a less appropriate than in gas phase combustion [31,32] and extensions proposed by Ge and Gutheil [31] could be better. Because only the standard β-function is available in ANSYS-Fluent and because for the purpose of comparative study of impact of different co-flow conditions on HiTAC conditions the difference is not expected to be large we have not explored those extensions.

3.4. NO_X model

Since the fuel, i.e. ethanol, used in the present study contains no nitrogen, NO_X formation mainly consists of thermal NO_X and N_2O intermediate mechanism [33–35]. Although prompt NO_X is also taken into account in the simulation, our numerical results have shown that it has little contribution to the total NO_X formation. This was also observed by other researchers [36].

Thermal NO_X is calculated by the extended Zeldovich mechanism [37,38], containing the following reactions governing the formation of thermal NO_X from molecular nitrogen:

$$O + N_2 \overset{k_1}{\leftrightarrow} N + NO \tag{11}$$

$$N + O_2 \overset{k_2}{\leftrightarrow} O + NO \tag{12}$$

$$N + OH \overset{k_3}{\leftrightarrow} H + NO \tag{13}$$

These reactions are considered to be reversible and the rate constants with units of $(m^3/mol{\cdot}s)$ are as follows:

$$\begin{aligned} k_{f,1} &= 1.8\times10^8 e^{-38370/T} & k_{r,1} &= 3.8\times10^7 e^{-425/T} \\ k_{f,2} &= 1.8\times10^4 T e^{-4680/T} & k_{r,2} &= 3.81\times10^3 T e^{-20820/T} \\ k_{f,3} &= 7.1\times10^7 e^{-450/T} & k_{r,3} &= 1.7\times10^8 e^{-24560/T} \end{aligned} \tag{14}$$

where “f” and “r” in superscript denotes forward and reverse rates, respectively. T means temperature in Kelvin.

In order to compute the NO concentration, concentrations of nitrogen radical [N], oxygen radical [O] and hydroxyl radical [OH] must be known.

Concentrations of [N] can be assumed in a quasi-steady state according to its nearly immediate consumption after creation. This N-radical formation is the rate limiting factor for thermal NO production, due to the extremely high activation energy of nitrogen molecule dissociation, which is caused by a triple bond between two nitrogen atoms as shown in Eq. (11). Hence the NO formation rate $(m^3/mol{\cdot}s)$ becomes:

$$\frac{d[NO]}{dt} = 2k_{f,1}[O][N_2]\frac{\left(1-\frac{k_{r,1}k_{r,2}[NO]^2}{k_{f,1}[N_2]k_{f,2}[O_2]}\right)}{\left(1+\frac{k_{r,1}[NO]}{k_{f,2}[O_2]+k_{f,3}[OH]}\right)} \tag{15}$$

Concentration of [O] and [OH] (mol/m^3) can be described by following partial equilibrium approaches [39–41]:

$$[O] = 36.64T^{1/2}[O_2]^{1/2}e^{-27123/T} \tag{16}$$

$$[OH] = 2.129\times10^2 T^{-0.57}e^{-4595/T}[O]^{1/2}[H_2O]^{1/2} \tag{17}$$

The formation of N_2O intermediate mechanism takes into account two reversible elementary reactions:

$$N_2 + O + M \leftrightarrow N_2O + M \tag{18}$$

$$N_2O + O \leftrightarrow 2NO \tag{19}$$

where M is a general third body.

N_2O can be assumed to be at quasi-steady-state, and the rate of $[N_2O]$ and the rate of NO_X formation via the N_2O-intermediate mechanism are:

$$[N_2O] = \frac{k_{f,1}[N_2][O][M] + k_{r,2}[NO]^2}{k_{r,1}[M] + k_{f,2}[O]} \tag{20}$$

$$\frac{d[NO]}{dt} = 2(k_{f,2}[N_2O][O] - k_{r,2}[NO]) \tag{21}$$

where

$$\begin{aligned} k_{f,1} &= 4.44\times10^{32}T^{-8.358}e^{-28234/T} & k_{r,1} &= 4.00\times10^8 e^{-28234/T} \\ k_{f,2} &= 2.90\times10^7 e^{-11651/T} & k_{r,2} &= 1.45\times10^{-29}T^{9.259}e^{-11651/T} \end{aligned} \tag{22}$$

In which the units of k_f,1 is $m^6/mol{\cdot}s$ while the other constants have the units of $m^3/mol{\cdot}s$. The transport equation for mean mass fraction of NO is solved with the mean source term obtained using the PDF of temperature fluctuations. As alternative to the determination of OH and O from partial equilibrium assumptions, they could be retrieved from the flamelets. However due the assumption made above in the non-adiabatic flamelet computation that the species concentration in the flamelets is independent of the heat loss, with only temperature changing when enthalpy changes, the procedure using the values from

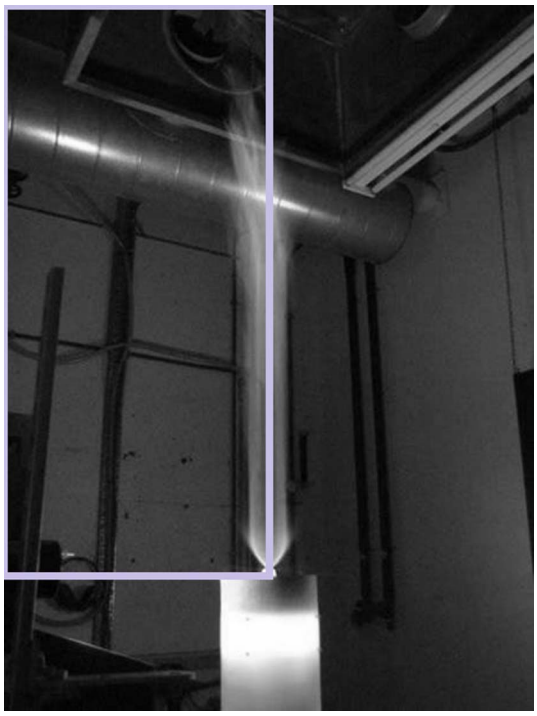

Fig. 2. The Delft spray flame (1500 K, 9% O_2; frame: computational domain).

partial equilibrium probably provides the more accurate NO source term.

4. Boundary conditions for modelling

The computational domain is illustrated in Fig. 2, which gives an image of a typical experimental flame. Further illustration of the computational domain, including spray angle (SA) and dispersion angle (DA) of the fuel spray are given in Fig. 3. As discussed in our previous investigation [12], SA needs to be analyzed for the estimation of spray trajectory based on measured droplet concentration at various heights. Since in the current comparative study the focus is on the influences of co-flow temperature and O_2 concentration in the co-flow on combustion characteristics, we use the design angle of 60° according to manufacturing data for all cases. DA is a presumed angle according to previous modelling [12], in which 10° is used and it is kept the same for all cases.

As shown in Fig. 3, ambient air is taken into account in order to investigate its influence on the spray combustion. The ambient air is entrained by the co-flow coming out from the pre-combustor, and may penetrate the co-flow and take part in the combustion process. The condition in which the spray combustion is most likely influenced by the ambient air is the one whose co-flow characteristics have the largest gradients with the ambient air (300 K and with 21% vol of O_2), i.e. the largest differences of O_2 concentration, temperature and velocity.

Table 1
Boundary conditions of the ethanol spray.

Fuel type	Ethanol
Fuel flow rate	0.383 g/s
Fuel temperature	303 K
Injection pressure	700 kPa
Spray angle	30°
Dispersion angle	10°
Sheet constant	12
Inner diameter	0.21 mm

In the present study, we keep the velocity of the co-flow at 3.5 m/s and vary the O_2 concentration (6%, 9%, 12%, 15%, 18% and 21% vol) and temperature (300 K, 600 K, 900 K, 1200 K and 1500 K) of the co-flow. As a result, the spray flame, which has 6% O_2 in the co-flow with a temperature of 1500 K, is most likely to be influenced by the ambient air.

The ethanol spray characteristics are kept the same in various cases, as shown in Table 1. There is always sufficient oxygen amount for complete combustion. Besides, the various amount of H_2O and CO_2 in co-flow in actual conditions are replaced by N_2 for the current comparative study.

In order to investigate the influence of the ambient air on the spray combustion, we applied different hydraulic diameters of the ambient air inlet, ranging from 6 to 14 times diameter of the co-flow inlet. This was done for the simulation of the case with 1500 K and 6% O_2 in the co-flow. With the employed vertical height of 2.5 m for the computational domain, we found that when the outer diameter of ambient air inlet is smaller than 8 times the outer diameter of the co-flow inlet, the back flow through the defined lateral outlet cannot be avoided and the computational stability is reduced. When diameter is larger than 12 times the diameter of the co-flow inlet, the recirculation zone caused by the co-flow and the back flow through the defined top outlet also increase the instability of the calculation. Therefore, a hydraulic diameter of 1600 mm (10 times the diameter of the co-flow inlet) is used in the present study and it results in relatively smooth streamlines of airflow. It must be noted that in the simulation there is a part of the ambient air is remaining laminar. This aspect has been studied by considering and comparing four different flow speeds (i.e. 0.1 m/s, 0.05 m/s, 0.025 m/s,

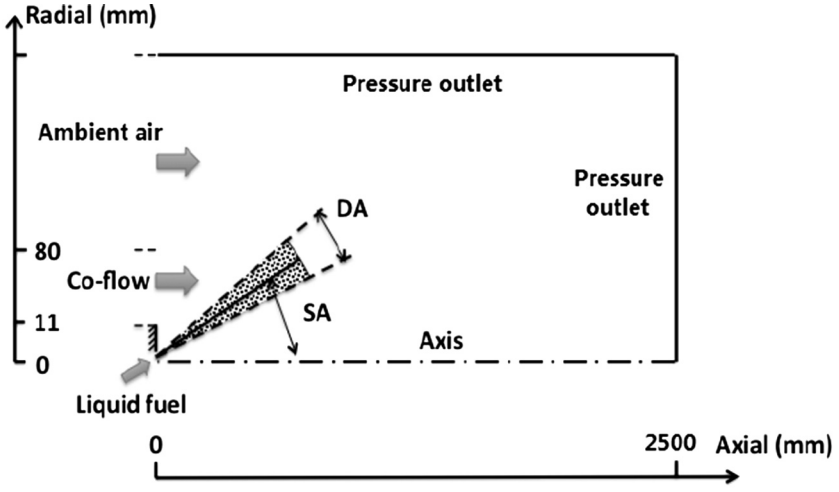

Fig. 3. Schematic of computational domain (SA: Spray Angle, DA: Dispersion Angle).

0.01 m/s) of the ambient air. The predicted velocity components and temperature show minor difference at various elevations. As a result, the ambient air shows minor influence on the spray combustion characteristics and the steady laminar flamelet combustion model can be applied.

5. Results and discussion

In this section two typical conditions, cold co-flow condition (300 K, 21% vol O_2) and hot co-flow condition (1500 K, 6% vol O_2) are compared to the closest conditions from experiment in this section. They represents spray flames under conventional condition and towards-HiTAC condition, respectively. Following that, the influences of O_2 and temperature in the co-flow are discussed.

5.1. The HiTAC condition and preliminary validation of models

Among the cases with various co-flow conditions, only several are feasible to be carried out in the experiment. The co-flow in the experiment is generated by the secondary burner located in the middle of the setup (see Fig. 1.). The O_2 concentration and the temperature of the co-flow are dependent on the inlet conditions of this burner. The validation of numerical data is done for the spray flames with hot co-flow and with cold co-flow. The former represents a HiTAC-like combustion regime whereas the latter is a conventional spray flame. In the simulation, 300 K and 21% vol O_2 condition is used for the cold co-flow condition, and 1500 K and 6% vol O_2 for the hot co-flow condition. In both, the co-flow velocity and the mass flow rate of ethanol are kept the same. In the experiment however, it is not possible to maintain the co-flow velocity the same and neither the exact matching of the mass flow of ethanol due to the limitation of the mass flow control and influence of high temperature on the atomizer. Besides, as discussed in our previous study [12], the trajectories of the spray need to be analyzed from the experiment in order to obtain good matching of SMD distribution between the experiment and simulation. As a result, the validation in the present study is mainly focused on the flame profile, and the range and trend of SMD at various elevations as discussed below.

Fig. 4 shows the experimental flames (LHS) and temperature contours of corresponding numerical solutions (RHS). The conventional flame is luminous and shows experimentally a low frequency oscillation, while the flame in hot co-flow turns into bluish and is very stable. The average temperature field in the present study, for both of the two cases present high similarities between the simulation and the experiment. In hot co-flow, the flame becomes “flameless” and shows the features of the HiTAC condition. Even though the input enthalpy of the hot co-flow is much higher than that of the cold co-flow, the predicted peak temperature is about 100 K lower than in the cold co-flow (1790 K). This can be attributed to the enlarged flame zone produced by the flame with low O_2 concentration co-flow, which results in a more uniform temperature distribution. Since the NO_X formation is mainly dependent on the peak temperature zone, the lower peak temperature in hot co-flow leads to a remarkably reduced NO_X emission as shown in Fig. 18.

Fig. 5 shows the predicted SMD of the drops at different elevations for the conventional flame. The experimentally measured SMD under similar conditions is shown in Fig. 6. In the numerical simulation, the SMD ranges from 5 μm to 40 μm at height z = 10 mm, and gradually changes to the range from 10 μm to 50 μm at height z = 40 mm. The measured data show a range from 12 μm to 38 μm at height z = 10 mm, and it changes to a range from 18 μm to 52 μm at height z = 40 mm. The predicted SMD matches the experimental data in the region of high droplet density, which is approximately in the middle of the range at each elevation. The trend of the SMD at each elevation also shows similarity between the simulation and the experiment. However, the range of radial locations of the SMD in the simulation is narrower than those in the experiment. This is attributed to two reasons. Firstly,

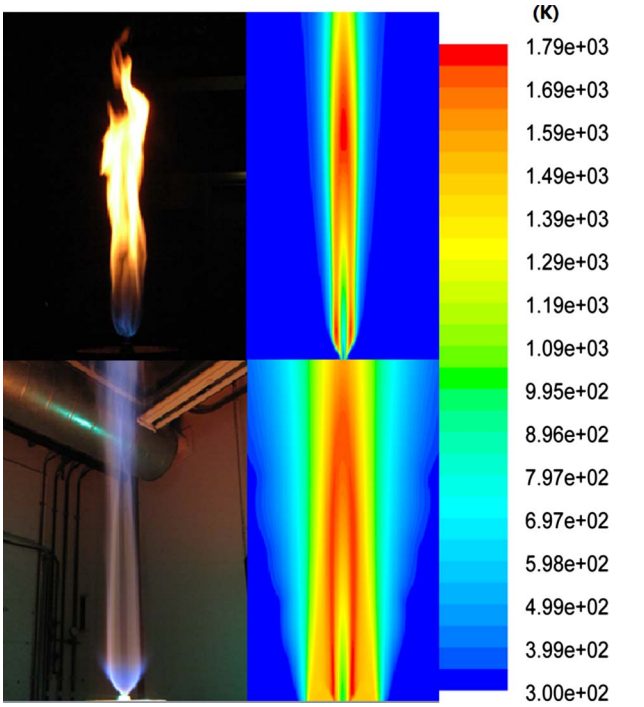

Fig. 4. Pictures of two flames (left) and the predicted temperature contours (right) (Above: 300 K, 21% O_2 co-flow; below: 1500 K, 6% O_2 co-flow).

as what we observed in the experiment, even at higher elevations, some small droplets still exist in the near center area, while few droplets are found in this region in the simulation. Both the low co-flow velocity of 0.29 m/s in the experiment, and the spray model in the simulation can be the causes of the difference. Secondly, we used an atomizer inner diameter of 0.21 mm (see Table 1) in the simulation according to the nozzle design. As we discussed in [12], this parameter is often larger than the design value and it requires further analysis in a specific case. With an adjusted inner diameter, the predicted SMD is supposed to spread in a wider range of radial position and match better with the measured data. Nonetheless, in the present study we keep the inner diameter as a constant of 0.21 mm for comparative investigation.

It is observed that the conventional ethanol spray flame is a diffusion flame, and its main body is attached to the spray by a triple flame composed of a rich premixed flame where the droplets are vaporizing and two lean premixed flames on both sides of the jet, as reported by Ruetsch et al. in [42].

The predicted and measured SMD of the droplets in hot co-flow conditions at various elevations are shown in Figs. 7, and 8,

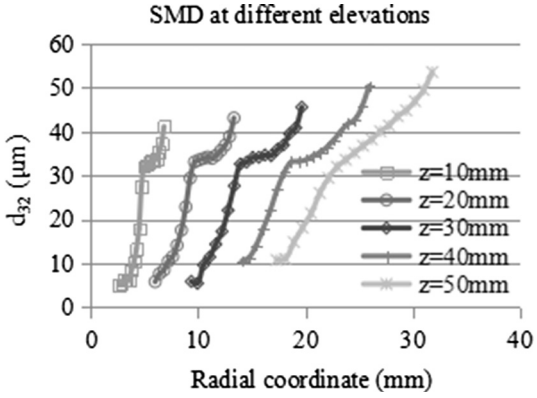

Fig. 5. Predicted SMD at various elevations in the case with 21% O_2 and 300 K co-flow condition (ethanol mass flow rate: 0.383 g/s; inlet co-flow velocity: 3.5 m/s; inner diameter of the spray: 0.21 mm).

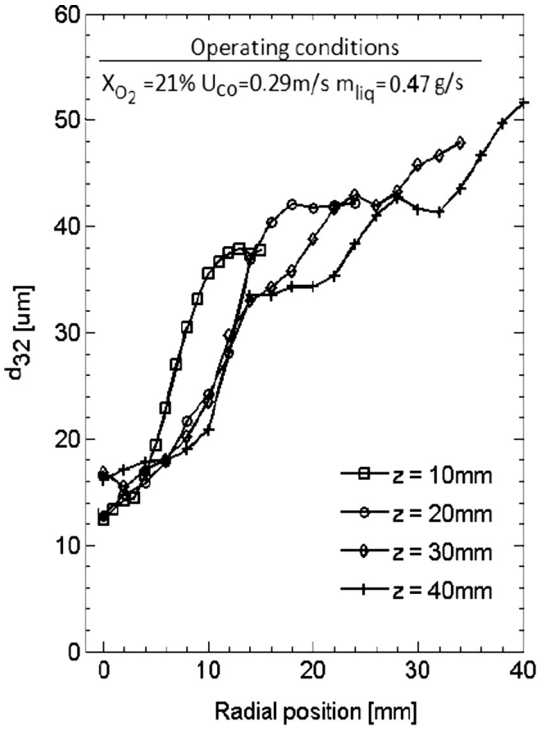

Fig. 6. Measured SMD at various elevations in the case with 21% O_2 and ~300 K co-flow condition.

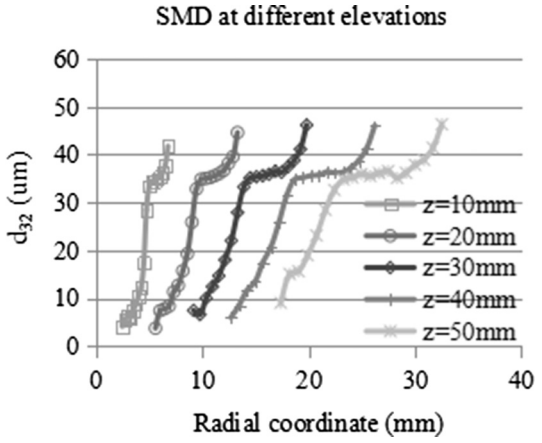

Fig. 7. Predicted SMD at various elevations in the case with 6% O_2 and 1500 K co-flow condition (ethanol mass flow rate: 0.383 g/s; inlet co-flow velocity: 3.5 m/s; inner diameter of the spray: 0.21 mm).

respectively. At height z = 10 mm, the SMD range and distribution is almost the same as for the conventional flame (i.e. with 21% O_2 and 300 K co-flow conditions). However, in the experiment the small droplets we observed in the conventional flame at higher elevations do not exist in the near-center-line area, but at larger radial locations. This makes the match of simulation results and experimental data of SMD distribution better than the conventional flame. Differently from the conventional conditions, the peak values of SMD at high elevations in hot co-flow do not increase gradually, but they are keeping the same value of approx. 40 μm. Both simulation and experiment show the same phenomena.

In the experiment, the data were measured at elevation z = 10 mm, 20 mm, 30 mm and 35 mm. At higher elevations the droplet number density drops and thus it is more difficult to measure accurately the SMD distribution. However, the less "steep" trend at a higher elevation in hot co-flow conditions shown in the experiment is predicted by the

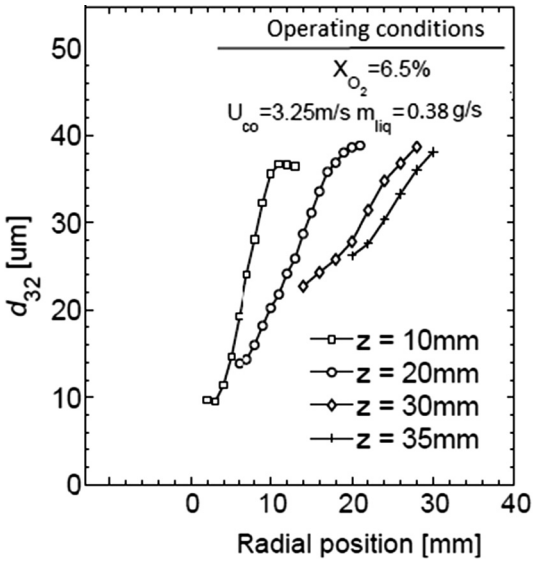

Fig. 8. Measured SMD at various elevations in the case with about 6.5% O_2 and 1480 K co-flow condition.

simulation with results at further elevations z = 40 mm and 50 mm. Besides, the left and right ends, which represent small droplets and large droplets, will be discussed in next section with the analysis of droplet number density. It is reasonable for the simulation to predict those small amount of droplets, while in the experiment they are not taken into account due to the Phase Doppler Anemometry (PDA) measuring.

The ethanol spray flame in hot co-flow exhibits a clear conical shape. The relatively larger cone observed in the experiment, compared to the conventional flame, is shown also in the simulation. Based on the obtained results it can be concluded that there is a good match between experimental and numerical data. In further study the ethanol spray flame is investigated under various co-flow conditions. Those results are presented and discussed in the following sections.

5.2. Influence of co-flow temperature

In this section, the volume fraction of oxygen in the co-flow is kept constant at 21% and the velocity of the co-flow is kept at 3.5 m/s. The predicted temperature contours of the ethanol spray flames under 300 K, 900 K and 1500 K co-flow conditions are presented in Fig. 9.

In all these conditions, an inner low temperature zone in the flame is observed. With the increase of co-flow temperature from 300 K to 1500 K, the peak temperature rises from 1809 K to 2267 K. The volume of peak temperature zone increases and it extends downstream. As a consequence, the high temperature of co-flow does not lead to a HiTAC condition, but increases the peak temperature and thus the thermal NO_X formation. In many other HiTAC applications, a high temperature of combustion air can result in a more uniform temperature distribution and a lower peak temperature. That is due to the increased velocity of combustion air under high temperature conditions. The high velocity leads to a larger amount of entrainment of flue gas, and thus creates a low O_2 concentration "co-flow", leading to a HiTAC-like condition. By increasing the velocity of the fuel, which can enhance the entrainment of flue gas as well, the HiTAC condition is also achievable for gaseous fuel [43].

Fig. 10 shows the axial velocity contours under 300 K and 1500 K co-flow conditions. A higher local velocity of co-flow near the fuel injection is found under 1500 K co-flow condition. This is attributed to increased fuel evaporation rate of the droplets under high co-flow temperatures. The fuel evaporation rate changes can be validated by the droplet number density and SMD distribution below.

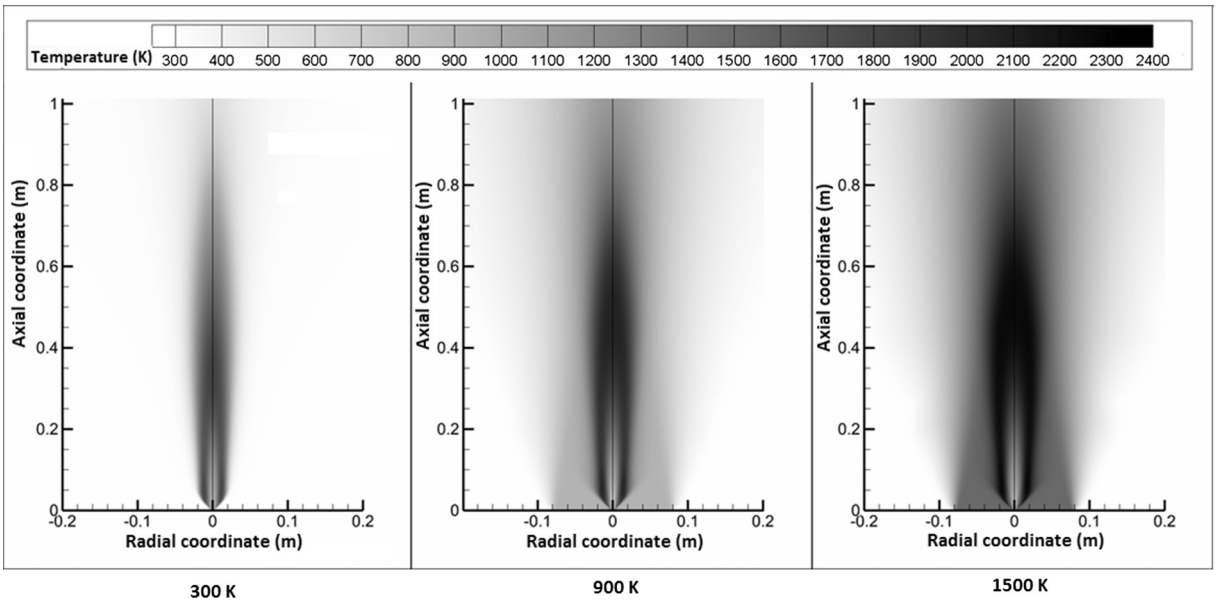

Fig. 9. Temperature contours of ethanol spray flames with different co-flow temperatures at constant velocity 3.5 m/s and at constant O_2%vol 21%).

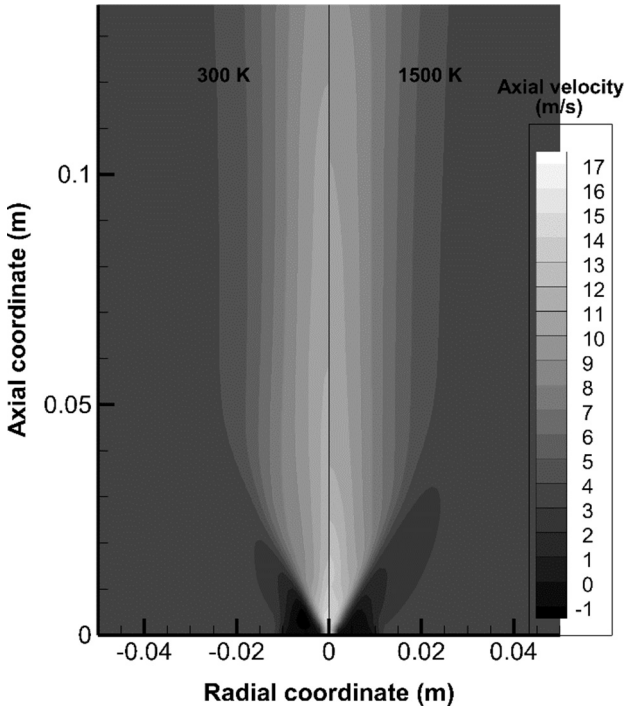

Fig. 10. Axial velocity contours under 300 K and 1500 K co-flow conditions (m/s).

Fig. 11 shows the droplet distribution at various elevations under 300 K, 900 K and 1500 K co-flow conditions. Below the height of z = 20 mm, the droplet concentration is alike for all investigated conditions. Further downstream, it can be noticed that the droplets evaporate faster under high temperature co-flow conditions. In 300 K co-flow case some droplets still exist at the height of z = 400 mm and at large radii, while very few droplets can be found already at z = 100 mm under 900 K and 1500 K cases, and no droplet found at radial locations larger than 0.06 m. This is confirmed by the experiment, where it has been observed that some droplets escape from the flame under cold co-flow conditions, while this is not seen under hot co-flow conditions. The simulation results show that the droplets present at large radii have the possibility to escape under low temperature co-flow conditions. Under 900 K and 1500 K co-flow conditions, the droplets reach the boiling temperature very fast due to the presence of hot co-flow at radii larger than 0.02 m. The evaporation rate is then mainly dependent on the liquid-vapor equilibrium around the droplets. As a result, at radii smaller than 0.03 m, the droplet concentration under 900 K and 1500 K is similar, whereas at larger radii, the droplets evaporate and disappear faster with the presence of 1500 K co-flow.

The SMD trend at downstream elevations is shown in Fig. 12. The peak in SMD values increases at higher downstream elevations for the 300 K co-flow conditions. This effect is caused by rapid evaporation of small droplets. However, for the high temperature co-flow, at each high elevation (radii above 0.02 m from where co-flow affects effectively) both large and small droplets decrease their size quickly and simultaneously, especially at locations of low droplet number density. This results in the vanishing of small droplets inside the spray cone and large droplets outside of the cone at each high elevations. Compared to the 900 K case, the droplets at high elevations (e.g. z = 90 mm) evaporate faster in 1500 K co-flow, and the SMD values in the middle of the profile, where a relatively large droplet number density exists, decrease from about 34 μm to about 30 μm. The profiles for both 900 and 1500 K are a bit wrinkled since a much lower amount of droplets exists at high elevations (see Fig. 11) and thus the statistical error in the captured samples can cause noticeable fluctuations.

Once the evaporated fuel meets the co-flow, a combustion process occurs. The O_2 concentration contours under 300 K and 1500 K co-flow conditions are presented in Fig. 13. A high temperature of co-flow accelerates the combustion process, whereas the low density of co-flow has a positive effect on enlarging the combustion zone. As a result, although the peak temperature increases adequately to the co-flow temperature, the temperature difference between the peak temperature and the co-flow temperature decreases. The increment of peak temperature from the case with 300 K co-flow to 1500 K, is only 458 K (from 1809 K to 2267 K), much less than the increase of absolute co-flow temperature, i.e. 1200 K (from 300 K to 1500 K).

5.3. Influence of O_2 concentration in the co-flow

In the present study, the applied co-flow conditions resemble properties of combustion air mixed with flue gas, i.e. high temperature and low oxygen concentration. The simulation results discussed in the previous section, indicate that although the decreased density of co-flow (due to a higher temperature) enlarges the flame zone, the increased enthalpy input still results in a higher peak temperature in the

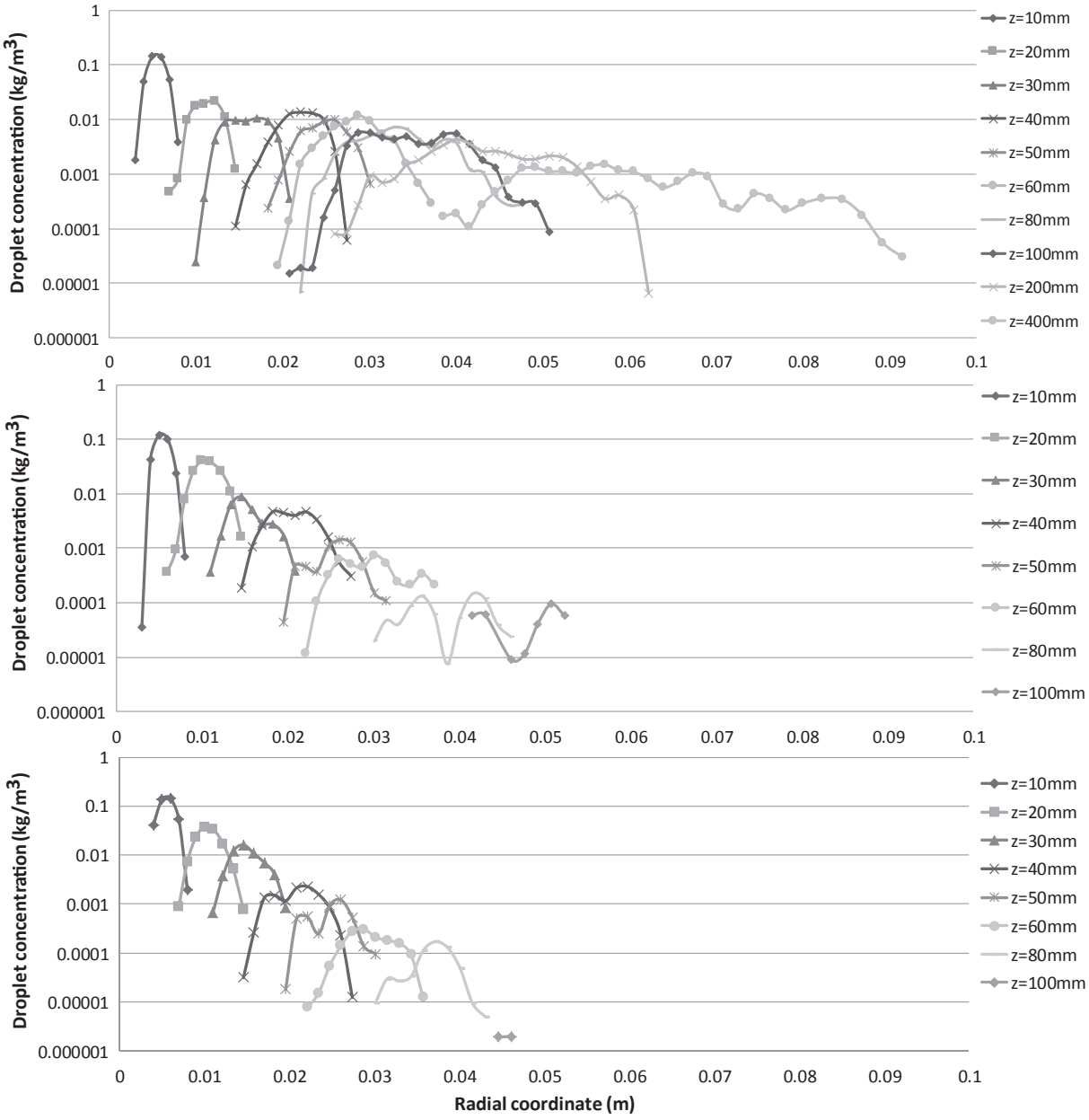

Fig. 11. Droplet concentration at various elevations under different co-flow temperatures (from top: co-flow temperature: 300 K, 900 K, 1500 K; velocity: 3.5 m/s; O_2%vol: 21%).

flame and thus leads to more thermal NO_X formation. Additionally, a higher co-flow temperature also accelerates the evaporation of droplets along the spray trajectories, which has negative effect on the "delay" of combustion and creating HiTAC-like conditions. Since various studies of HiTAC on gaseous fuel show that the combination of an increased temperature and a lowered O_2 concentration, which is created by entraining flue gas with combustion air/fuel, leads to HiTAC condition, we further investigate the effect of O_2 concentration in the co-flow on spray combustion in this section.

Fig. 14 shows the predicted average temperature and O_2 concentration contours of the ethanol spray flames under 18%, 12% and 6% volume fraction of O_2 co-flow conditions. The co-flow temperature is kept at 1500 K and the co-flow velocity remains 3.5 m/s. The peak temperature decreases from 2175 K to 1705 K and 1689 K with reduction of O_2 concentration from 18% to 12%, and to 6% in the co-flow, respectively. An enlargement of combustion zone is also found. Compared to the co-flow temperature, 1500 K, the temperature difference in the flame has been reduced from 675 K to 205 K, and to 189 K.

SMD of the drops and their concentration profiles at different elevations under various co-flow O_2 concentrations (18%, 12% and 6%) are presented in Figs. 15and 16, respectively. According to Fig. 15, with the decrease of O_2 concentration in the co-flow, the SMD profile at z = 90 mm is less wrinkled. As we discussed before, the wrinkled profile is mainly due to the low droplet concentration. Thus more droplets still exist at that elevation with a lower O_2 concentration co-flow. This is also visible from Fig. 16. Besides, SMD values at location of high droplet concentration for cases with 1500 K and 21%vol O_2 concentration are generally lower than those comparable data for cases of 1500 K and low O_2 content.. This indicates that the evaporation process has been reduced for the low O_2 concentration co-flow. This is confirmed further by the droplet concentration distribution shown in Fig. 16. At elevations z = 10 mm and 20 mm in Fig. 16, the droplet concentration is similar for various O_2 co-flow conditions. From z = 30 mm, it is clear that more droplets survive in a lower O_2 concentration co-flow. As a result, when the evaporated fuel mixes with the co-flow containing a lower O_2 concentration (18%, 12% and 6% co-

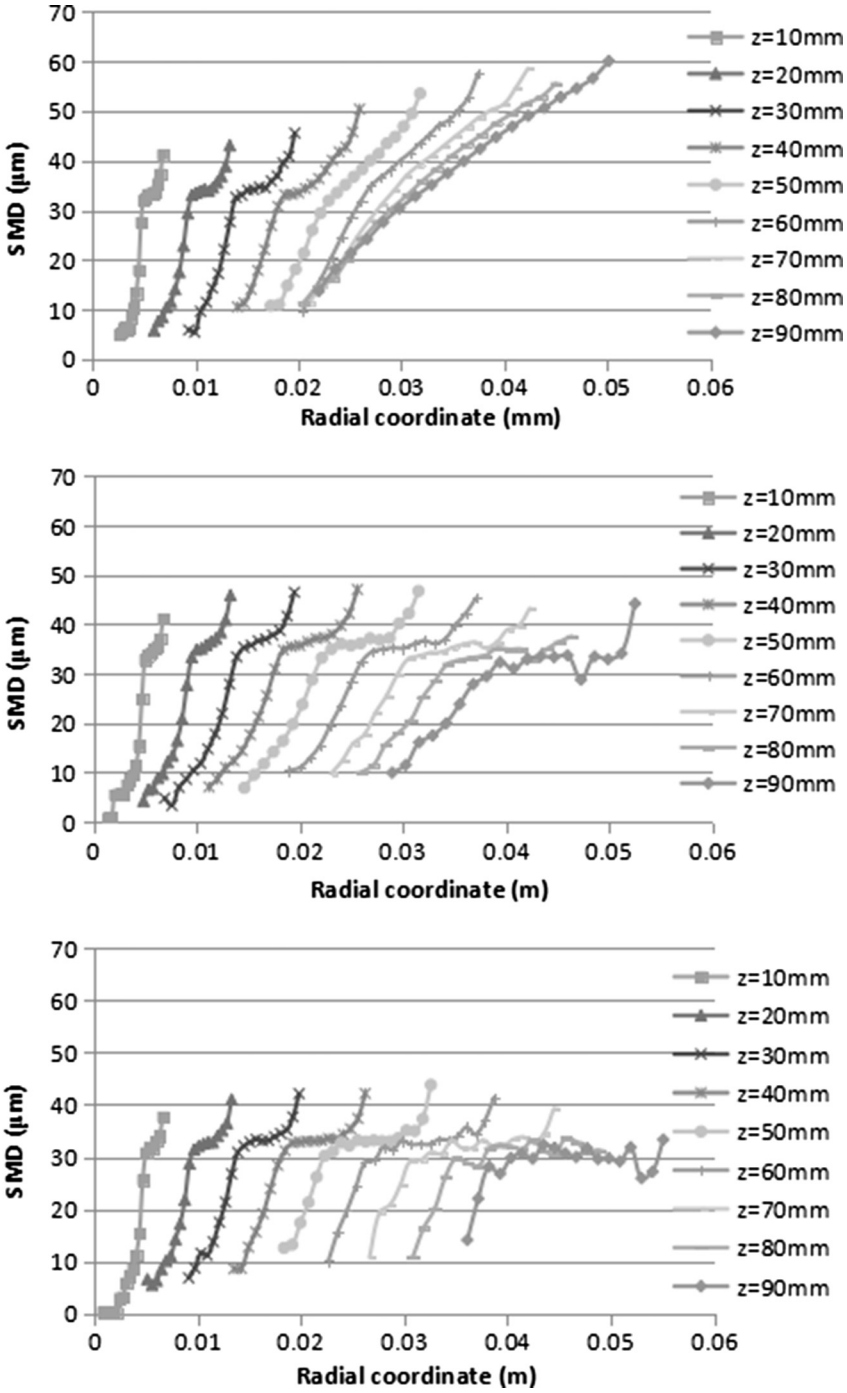

Fig. 12. SMD at various elevations under different co-flow temperatures (from top: co-flow temperature: 300 K, 900 K, 1500 K; co-flow velocity: 3.5 m/s; O_2%vol: 21%).

flow O_2%vol), this leads to a lower peak temperature in the flame and a reduced consumption of fuel. This combined with a lowered temperature in return slows down the evaporation process of droplets. Thus the volume of combustion zone increases creating a HiTAC-like condition. Based on previous observation, i.e. that a high temperature co-flow leads to a high peak temperature in the flame, we concluded that in the combination of a high temperature and a low O_2 concentration in the co-flow, which can lead to HiTAC- like conditions, reducing the O_2 concentration is the dominant factor for decreasing the peak temperature in the flame. However, the combustion process is continuously consuming O_2. If no sufficient O_2 in the low O_2 co-flow can be provided for the combustion process, some other process like secondary cracking can occur and soot formation can be increased as well. For gaseous fuels, velocity components or locations of fuel injection can be tuned in a relatively simple way to mix fuel with low O_2 concentration co-flow (mixture of combustion air and flue gas). Spray flames have a fuel-rich zone along or confined by the spray, which makes the mixing more difficult to be optimized towards HiTAC conditions. The optimization needs to be carried out based on the analysis of a specific fuel in order to create a HiTAC-like condition.

Fig. 17 shows the peak temperatures in the cases with different O_2 concentration at various co-flow temperature conditions. Each point represents one test case. The condition with a temperature of 300 K and 6%vol O_2 in the co-flow is beyond the lean flammability limit. Under constant co-flow temperature regime, the peak temperature is reduced when the O_2 concentration in the co-flow decreases. Besides, the temperature difference between the peak and co-flow temperature drops with the reduced O_2 concentration in the co-flow.

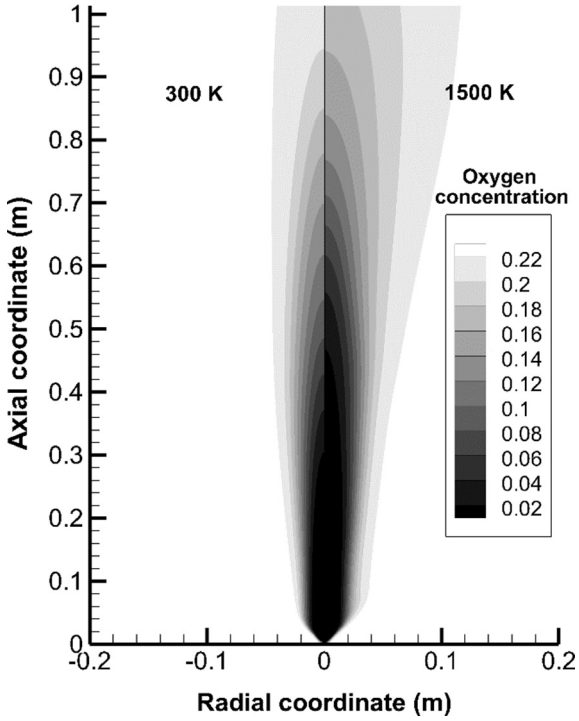

Fig. 13. O2 concentration contours under 300 K and 1500 K co-flow conditions (mass fraction)(co-flow velocity: 3.5 m/s; O_2%vol: 21%).

For the same co-flow O_2 concentration, the peak temperature increases with an increase of co-flow temperature. However, the temperature difference between the peak and co-flow temperatures decreases. As a result, among the investigated cases, the one with 6%vol O_2 concentration and 1500 K co-flow condition has the most uniform temperature distribution.

NO average mass fraction contours for conventional (300 K, 21%vol O_2 concentration) and HiTAC (1500 K, 6%vol O_2 concentration) flames are shown in Fig. 18. The former has a peak temperature of 1809 K and the latter of 1689 K according to the simulation results. The NO formation occurs mainly in the region with peak temperature, therefore it is suppressed under HiTAC regime. Considering the extra enthalpy input from the 1500 K co-flow, the NO formation is reduced considerably, since the peak temperature in the regular spray flame under co-flow temperature equal to that of the HiTAC, i.e. 1500 K and 21%vol O_2 concentration is 2267 K.

The peak temperature under various co-flow conditions is related to the flame volume. The flame volume can be explained with support of oxidation mixture ratio [44] in form of Eq. (23):

$$R_o = \frac{m_o}{m_o + \sum_c S_c m_{F,c}} \tag{23}$$

where $S = n_0 M_0 / n_F M_F$ with m the mass fraction, n the stoichiometric ratio, M the molar mass, and index O, F, C representing oxygen, fuel and flue gas respectively. Following [44] we assume that $R_0 = 0.99$ is representative for the external boundary of the flame and $R_0 = 0.01$ is representative for the internal boundary.

Fig. 19 shows the calculated flame volumes under various co-flow conditions. With the same co-flow temperature, when the O_2 concentration decreases in the co-flow, the ethanol spray flame volume is enlarged, especially in case when the O_2 concentration is lower than 12% vol. Since for the same co-flow temperature, the heat dissipated by the flame with a bigger volume (co-flow with reduced O_2 concentration) is absorbed via a larger combustion zone, the peak temperature in the flame decreases.

With the same constant O_2 concentration in the co-flow, the change in the flame volume caused by a high temperature co-flow is not sufficient to cover the local enthalpy increase in the system and thus the peak temperature is enhanced. For the co-flow with 6%vol and 9%vol O_2 concentrations, when the co-flow temperature increases, the flame volume is enlarged much more than in other O_2 concentration conditions. Since the co-flow velocity is the same for all investigated cases, the increment of enthalpy input due to co-flow with a higher temperature in all O_2 concentration conditions is almost the same. As a result, the ethanol spray flames in the co-flow with 6%vol and 9%vol O_2 concentrations have greater potential than other cases to reach HiTAC conditions. The HiTAC is related to the uniformity of the temperature distribution mainly, and also to the ignition temperature and adiabatic temperature for a specific fuel. Since the 1500 K and 6%vol O_2 concentration case has a peak temperature of 1689 K, with only a difference of 189 K from the co-flow temperature, and shows a “flameless” feature in the experiment, it is then considered to be the HiTAC condition.

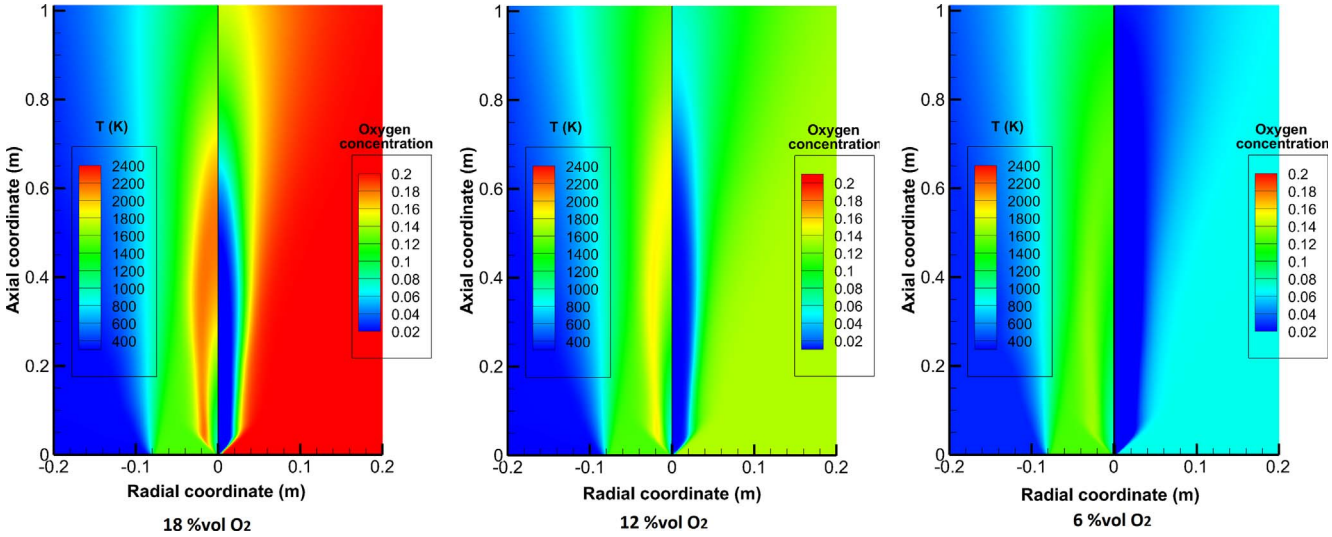

Fig. 14. Temperature (K) and O_2 concentration (mass fraction) contours with different co-flow O_2 concentration (left to right: co-flow O_2%vol: 18%; 12%; 6%; velocity: 3.5 m/s; T: 1500 K).

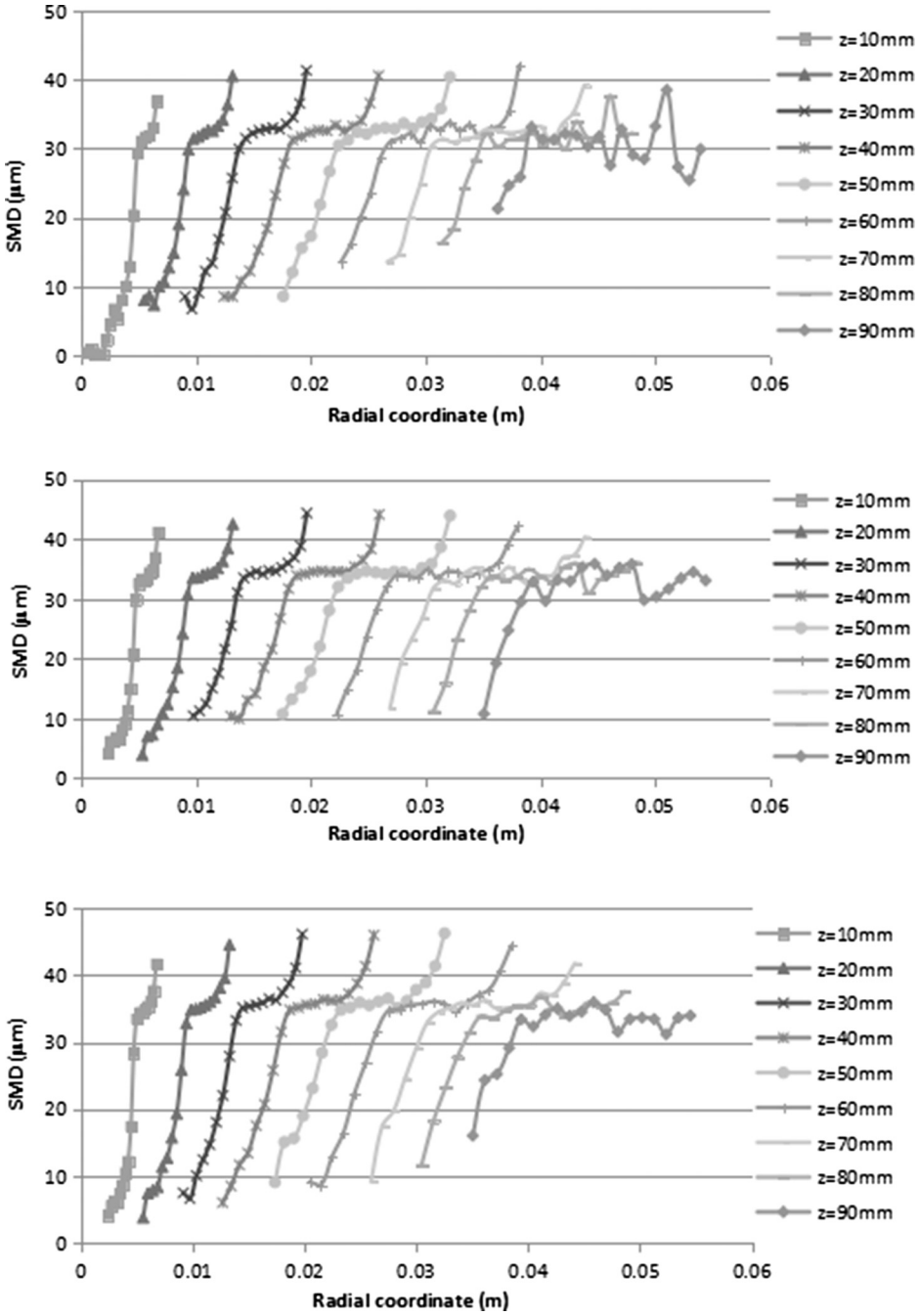

Fig. 15. SMD of droplets at various elevations under different co-flow O_2 concentration (from top: co-flow O_2%vol: 18%; 12%; 6%; velocity: 3.5 m/s; T: 1500 K).

6. Conclusions

We presented results of the numerical investigation of ethanol spray combustion under various co-flow conditions. The different temperature and O_2 concentration content in the co-flow were applied to mimic the mixing conditions of combustion air and flue gas. Their influence on the spray combustion was numerically studied in order to achieve HiTAC-like conditions with uniform temperature distributions and correspondingly low NO_X emissions. The present study was based on the analysis of the Delft Spray-in-Hot-Coflow (DSHC) experimental set-up and the operating conditions. The experiment was carried out in open space to allow for optical measurement. Thus our defined computational domain also contains the air flow of ambient air, although it was further found that the ambient air showed minor influence on the flame zone.

The numerical results of the cold co-flow case (300 K and 21%vol O_2 concentration) and the hot co-flow case (1500 K and 6%vol O_2 concentration) were compared with the experimental data under the similar co-flow conditions. Good match was shown on the flame profile, and the range and trend of SMD at various elevations. Some deviations were discussed and attributed to limitations of either the experiment or models used in simulation. Generally, good agreement between numerical and experimental data was achieved.

The simulation results showed that although the increased temperature leads to a lowered density of co-flow which then enlarges the flame zone, the increased enthalpy input still results in a high peak temperature in the flame and thus leads to more thermal NO_X formation. Moreover, a high co-flow temperature also accelerates the evaporation of droplets along the spray trajectories, which has negative effect on the “delay” of combustion and creation of HiTAC-like conditions. However, the temperature difference between the peak temperature and the co-flow temperature decreases with the increased co-

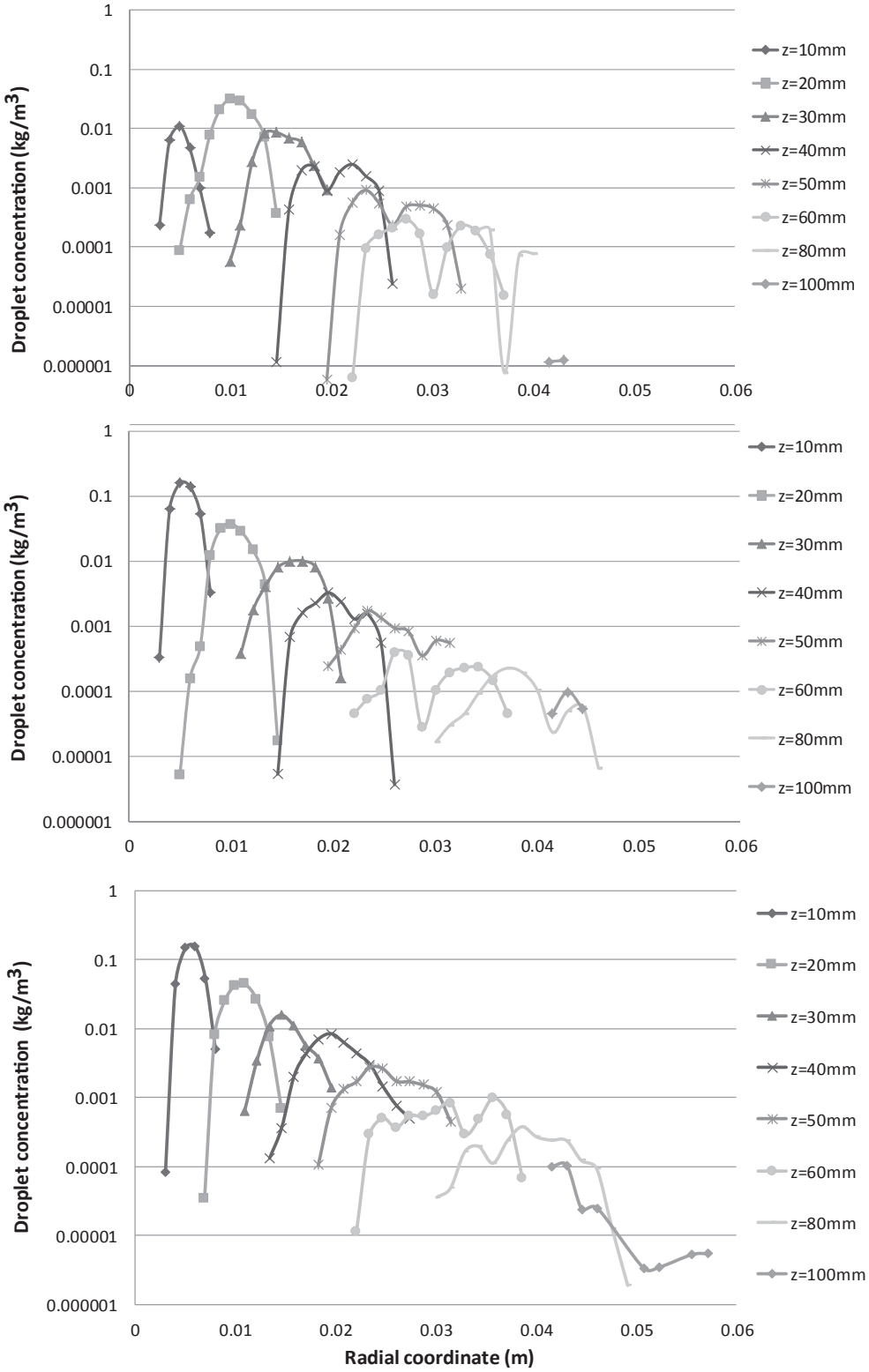

Fig. 16. Droplet concentration at various elevations under different co-flow O_2 concentration (from top: co-flow O_2%vol: 18%; 12%; 6%; velocity: 3.5 m/s; T: 1500 K).

flow temperature.

In some HiTAC applications with gaseous fuels, a high temperature of combustion air can result in a more uniform temperature distribution and a lower peak temperature. This is due to the increased velocity of combustion air under high temperature conditions, with which more flue gas is entrained and it creates a lower O_2 concentration "co-flow", leading to a HiTAC-like condition. According to previous research [43], increasing the velocity of the gas fuel can create the same situations and thus supports achieving the HiTAC conditions. However, if a larger amount of entrainment does not contain a relatively low O_2 concentration, it may strengthen the combustion process rather than reducing the peak temperature and thermal NO_X formation.

For ethanol spray flames, a lower O_2 concentration leads to a lower peak temperature in the flame and reduced consumption of fuel. Both in return slow down the evaporation process of droplets. Thus the combustion zone volume increases creating a HiTAC-like condition.

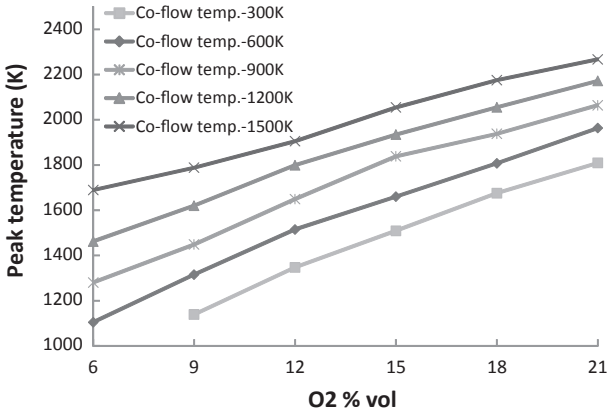

Fig. 17. Peak temperatures in various co-flow conditions.

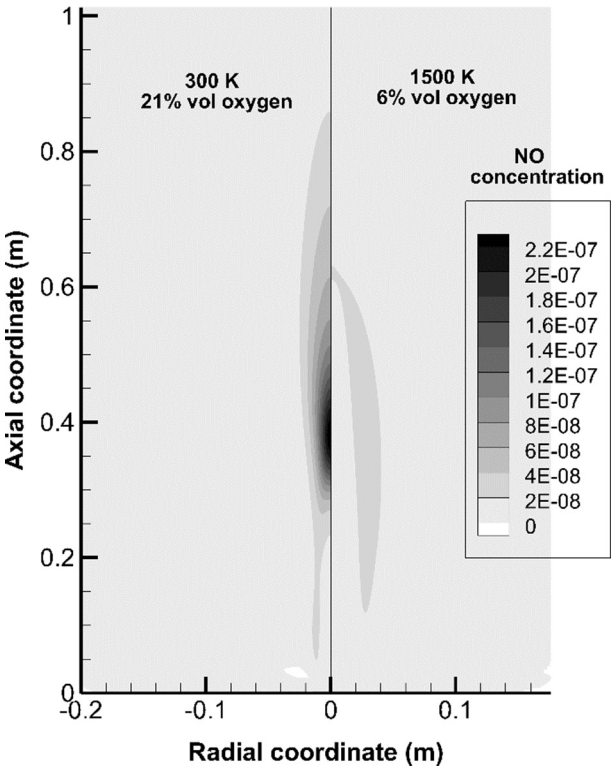

Fig. 18. NO mass fraction contours under conventional and HiTAC conditions.

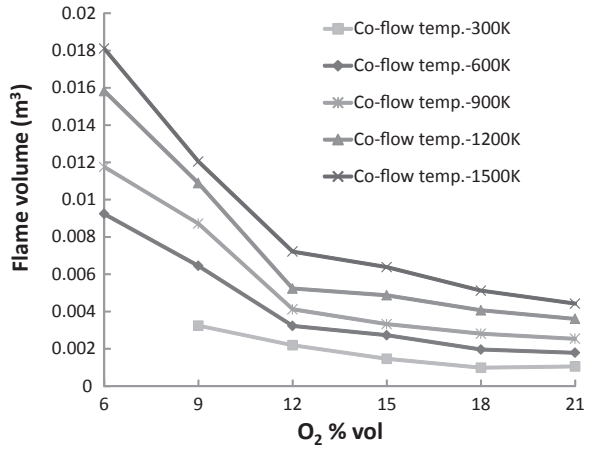

Fig. 19. Calculated flame volumes under various co-flow conditions.

The calculated flame volumes in various co-flow conditions were compared and discussed. The ethanol spray flames in the co-flow with 6%vol and 9%vol O_2 concentrations resembles the HiTAC flames mainly due to the considerable enlargement of combustion zone (the enthalpy input from high temperature co-flow remain similar). Since the 1500 K and 6%vol O_2 concentration case has a peak temperature of 1689 K, with only a difference of 189 K from the co-flow temperature, and shows a “flameless” feature in the experiment, it is then considered as a HiTAC condition.

For heavy fuel oils, the mixing process is more difficult to be optimized towards HiTAC conditions than light fuel oils. On one hand, the peak temperature can be reduced in a low O_2 concentration co-flow condition in spray flames; on the other hand, the even lower O_2 concentration condition created after combustion may lead to problems of secondary cracking, soot formation and flame extinction. The optimization needs to be carried out based on the analysis of a specific fuel in order to create a HiTAC-like condition.

Acknowledgements

The authors would like to thank for the support of the Technology Foundation STW, Stork Technical Services and Shell.

References

[1] Tsuji H, Gupta A, Hasegawa T, et al. High temperature air combustion: from energy conservation to pollution reduction. Boca Raton: CRC Press; 2002.
[2] Cavaliere M de Joannon. Mild combustion. Prog Energy Combust Sci 2004;30–4:329–66.
[3] Blarino L, Fantuzzi M, Malfa E, Zanusso U, Tenova. Flexytech burners: flameless combustion for very low NOx reheating furnaces. In: Proceedings of the HITAC conference, Thailand, 2007.
[4] Wünning JA, Wünning JG. Flameless oxidation to reduce thermal NO-formation. Prog Energy Combust Sci 1997;23(1):81–94.
[5] Arghode VK, Gupta AK. Development of high intensity CDC combustor for gas turbine engines. Appl Energy 2011;88(3):963–73.
[6] Blasiak W, Yang W. Volumetric combustion of coal and biomass in boilers. In: Proceedings of the HITAC conference, Thailand, 2007.
[7] Kunio Y. R & D commercialization of innovative waste-to-energy technologies. In: Proceedings of the HITAC conference, Thailand, 2007.
[8] Weber R, Smart JP, Kamp W vd. On the (MILD) combustion of gaseous, liquid, and solid fuels in high temperature preheated air. Proc Combust Inst 2005;30:2623–9.
[9] Schaffel-Mancini N, et al. Novel conceptual design of a supercritical pulverized coal boiler utilizing high temperature air combustion (HTAC) technology. Energy 2010;35(7):2752–60.
[10] Zhang H, et al. Development of high temperature air combustion technology in pulverized fossil fuel fired boilers. Proc Combust Inst 2007;31(2):2779–85.
[11] Jenny P, Roekaerts D, Beishuizen N. Modeling of turbulent dilute spray combustion. Prog Energy Comb Sci 2012;38:846–87.
[12] Zhu S, Roekaerts DJEM, Pozarlik A, Meer TH van der. Eulerian-Lagrangian RANS model simulations of the NIST turbulent methanol spray flame. Combust Sci Technol 2015;187(7):1110–38.
[13] Ma L, Zhu S, Rodrigues H, Tummers M, van der Meer T, Roekaerts D. Numerical investigation of ethanol spray-in hot-coflow flame using steady flamelet model. In: Proceedings of the 8th Mediterranean combustion symposium, Turkey, 2013.
[14] Ma L, Naud B, Roekaerts D. Transported PDF modeling of ethanol spray in hot-diluted coflow flame. Flow Turbulence Combust 2016;96(2):469–502.
[15] Ma L, Roekaerts D. Modeling of spray jet flame under MILD condition with non-adiabatic FGM and a new conditional droplet injection model. Combust Flame 2016;165:402–23.
[16] Rodrigues HC. Spray combustion in moderate and intense low-oxygen conditions -an experimental study, PhD thesis, Delft University of Technology, 2015.
[17] Correia Rodrigues H, Tummers MJ, van Veen EH, Roekaerts DJEM. Effects of coflow temperature and composition on ethanol spray flames in hot-diluted coflow. Int J Heat Fluid Flow 2015;51:309–23.
[18] Correia Rodrigues H, Tummers MJ, van Veen EH, Roekaerts DJEM. Spray flame structure in conventional and hot-diluted combustion regime. Combust Flame 2015;162:759–73.
[19] Gutheil E. Issues in computational studies of turbulent spray combustion, experiments and numerical simulations of diluted spray turbulent combustion. Merci B, Roekaerts D, Sadiki A, editors. Springer; 2011. p. 1–39.
[20] Schmidt DP, Nouar I, Senecal PK, et al. Pressure-swirl atomization in the near field. SAE Paper 01–0496, SAE, 1999.
[21] Han Z, Perrish S, Farrell PV, Reitz RD. Modeling atomization processes of pressure-swirl hollow-cone fuel sprays. Atomization Sprays 1997;7(6):663–84.
[22] Lefebvre H. Atomization and sprays. Hemisphere Publishing Corporation; 1989.
[23] Weber. Zum Zerfall eines Flüssigkeitsstrahles. ZAMM 1931;11:136–54.
[24] Taylor GI. The Shape and Acceleration of a Drop in a High Speed Air Stream.

Technical report, In the Scientific Papers of Taylor GI, editor, G. K. Batchelor, 1963.
[25] O'Rourke PJ. Collective Drop Effects on Vaporizing Liquid Sprays. PhD thesis, Princeton University, Princeton, New Jersey, 1981.
[26] Ranz WE, Marshall Jr. WR. Evaporation from drops. Part I Chem Eng Prog March 1952;48(3):141–6.
[27] Ranz WE, Marshall Jr. WR. Evaporation from drops. Part II Chem Eng Prog April 1952;48(4):173–80.
[28] Marinov NM. Kinetic model for high temperature ethanol oxidation. Int J Chem Kinet 1998;32:183–220.
[29] Muller CM, Breitbach H, Peters N, Partially Premixed Turbulent Flame Propagation in Jet Flames, Technical report, 25th Symposium (Int) on Combustion, The Combustion Institute, 1994.
[30] Binniger B, Chan M, Paczkko G, Herrmann M, Numerical Simulation of Turbulent Partially Premixed Hydrogen Flames with the Flamelet Model, Technical report, Advanced Combustion Gmbh, Internal Report, 1998.
[31] Ge H-W, Gutheil E. Probability density function (PDF) simulation of turbulent spray flows. Atomization Sprays 2006;16:531–42.
[32] Luo K, et al. Direct numerical simulations and analysis of three-dimensional n-heptane spray flames in a model swirl combustor. Proc Combust Inst 2011;33:2143–52.
[33] Glarborg P, Johnsson JE, Dam-Johansen K. Kinetics of homogeneous nitrous oxide decomposition. Combust Flame 1994;99:523–32.
[34] Barlow RS, Fiechtner GJ, Carter CD, Chen JY. Experiments on the scalar structure of turbulent CO/H2/N2 jet flames. Combust Flame 2000;120:549–69.
[35] Tabacco D, Innarella C, Bruno C. Theoretical and numerical investigation on flameless combustion. Combust Sci Technol 2002.
[36] Barrie Jenkins, Peter Mullinger. Industrial and process furnaces: principles, design and operation.
[37] Zeldovich JB. The oxidation of nitrogen in combustion and explosion. Acta Physicochimica 1946;21:577–628.
[38] Bowman CT, Seery DJ. Emissions from continuous combustion systems. New York: Plenum Press; 1972.
[39] Warnatz J. NOx formation in high temperature processes. Germany: University of Stuttgart; 2001.
[40] Baulch DL, Cobos CJ, Cox RA, et al. Evaluated kinetic data for combustion modelling. J Phys Chem Ref Data 1992;21:411–734.
[41] Westbrook CK, Dryer FL. Chemical kinetic modelling of hydrocarbon combustion. Prog Energy Combust Sci 1984;10(1):1–57.
[42] Ruetsch GR, Vervisch L, Linan A. Effects of heat release on triple flame. Phys Fluids 1995;7(6):1447–54.
[43] Zhu S, Chen L, Zhu T, Wu J. Effect of length-width ratio of the rectangular air-jet on NOX emission in HiTAC [J]. Ind Furnace 2005;27(6):4–8.
[44] Yang W, Blasiak W. Numerical study of fuel temperature influence on single gas jet combustion in highly preheated and oxygen deficient air. Energy 2005;30:385–98.